Charge transport in the normal state of electron- or hole-doped $YBa_2Cu_3O_{7-x}$

T. Doderer,* C. C. Tsuei, W. Hwang, and D. M. Newns
IBM Thomas J. Watson Research Center, P.O. Box 218, Yorktown Heights, New York 10598
(Received 11 February 2000)

By using a field-effect transistor configuration, we have demonstrated that it is possible to dope electrons or holes into an initially underdoped $YBa_2Cu_3O_{7-x}$ film at room temperature. The results of systematic measurements of the dual-type transconductance indicate comparable field-effect mobilities for electrons and holes. We propose a model based on band bending and localized electronic states within the band gap of the Mott insulator to explain the dual-type charge transport.

I. INTRODUCTION

One of the most outstanding characteristics of highly charge-correlated systems such as the cuprates is the strong doping dependence of their electronic properties.[1] A small amount of doping leads to a large suppression of the long-range antiferromagnetic (AF) ordered state and an ensuing Mott insulator to metal transition.[2] The study of the doping effect on various physical and chemical properties in cuprates is mostly achieved by varying the oxygen content, the cation substitution, or both. However, chemical doping is often limited by the solubility of a specific dopant in a given cuprate system. The experimentally established variations of the critical temperature T_c and the Néel temperature T_N with doping concentration n in cuprate systems such as the hole-doped LaSrCuO and the electron-doped NdCeCuO systems[3] suggest an electron-hole asymmetry. Such a conclusion is based on the characteristics of the T-n phase diagram in two different cuprate systems. In addition to the type of charge carriers (electrons or holes), structural or chemical subtleties could be responsible for the observed electron-hole asymmetry. Furthermore, the theoretical treatment of this topic is still controversial.[4,5] To help resolve these issues, it is important to study the effect of electron and hole doping in the same cuprate system.

In this work, we utilize a standard field-effect transistor (FET) configuration to introduce either holes or electrons by reversing the polarity of the applied electric field **E**. The FET technique is widely used in semiconductor devices.[6] In the case of high-T_c superconductors, FET or related techniques have been employed to study the influence of the **E** field on the superconducting properties such as T_c or the critical current density J_c.[7,8] In the undoped cuprates, a significant field-induced conductance enhancement at room temperature has recently been shown using $Y_{1-y}Pr_yBa_2Cu_3O_{7-x}$ (YPBCO) as the channel material.[9–11] However, we note that in all previous FET studies only hole doping was demonstrated.

In this work, we will show that it is feasible to inject electrons or holes into an underdoped cuprate such as YBCO, using an all oxide FET configuration. To study the electron-hole symmetry issue, we investigate the transconductance arising from the dual-type (electron or hole) electronic switching in the same underdoped Mott insulating cuprate.

II. SAMPLE FABRICATION

The inset of Fig. 1(a) shows schematically a typical electric-field-effect thin-film transistor (TFT) with a thin layer of chemically undoped $YBa_2Cu_3O_{7-x}$ (YBCO) as the channel. We use a single crystal of electrically conducting Nb-doped $SrTiO_3$ (Nb-STO) as the substrate (0.5 wt % Nb). A thin layer of undoped STO (400 nm thick) is deposited epitaxially on top of the substrate. It is followed by an optimally doped c-axis oriented YBCO (50 nm thick) layer grown epitaxially *in situ* on top of the STO layer. For both thin films we use pulsed laser deposition from stoichiometric targets in an oxygen atmosphere of 300 mTorr and a substrate temperature of 740 °C. The TFT is completed by electron-beam evaporation of the source (S) and drain (D) electrodes (Pt, 150 nm thick) through a Si stencil mask in a separate run. Finally, we isolate the individual devices on the

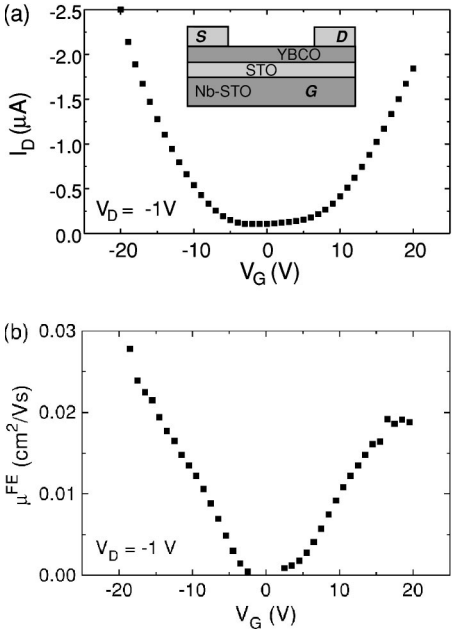

FIG. 1. (a) Dual-type transconductance curve of a YBCO thin film. For $V_G<0$ ($V_G>0$) p-type (n-type) charge transport is established. The inset of (a) shows a schematical drawing of the FET with source (S), drain (D), and gate (G) electrodes. (b) Field-effect mobility as a function of the gate voltage V_G numerically calculated from the data shown in (a).

chip by cutting trenches into the YBCO layer with a patterned laser beam. A single FET device typically has channel length $l=5\ \mu$m and width $w=90\ \mu$m. The measured STO film capacitance $C_s=5$ fF/μm^2 per unit area, and using the known STO film thickness we obtain an estimate of the dielectric constant $\epsilon_r \approx 230$ for the STO film at room temperature.

The deposition of a fully oxygenated layer of YBCO as the starting point is important in order to obtain an FET device with reproducible electronic characteristics. Oxygen in the channel is then removed through controlled annealing of the sample in Ar at a temperature of 250–350 °C for 1–2 h. It is well known that thermal annealing in an inert atmosphere removes the oxygen atoms from the Cu-O chains in YBCO, thus leaving the Cu-O planes intact and ensuring a channel of high crystal quality. This is crucial to achieve a high-field-effect mobility of the induced carriers. The detailed device characteristics, such as channel resistivity, carrier mobility, or transconductance, can be reproducibly and precisely controlled by such annealing procedures. The properties of the dielectric layer of STO does not deteriorate as a result of annealing.

III. EXPERIMENTAL RESULTS

With the device shown in the inset of Fig. 1(a), a gate voltage $V_G<0$ introduces holes into the bottom layer of the YBCO (*p*-type conductance), thus increasing its conductivity. The transconductance

$$g=\left.\frac{\partial I_D}{\partial V_G}\right|_{V_D=\text{const}} \tag{1}$$

is a measure of the gate voltage (V_G) dependence of the current I_D flowing between the source (always grounded) and drain electrodes, keeping the voltage V_D between source and drain constant. I_D is measured at room temperature versus V_G and V_D using a standard semiconductor parameter analyzer. As shown in Fig. 1(a), not only do we observe a pronounced transconductance for $V_G<0$ but also for $V_G>0$. For positive gate voltage, clear *n*-type channel behavior is observed in YBCO implying a finite electron mobility [Fig. 1(b)]. This has never been observed using chemical doping. Starting with the proper oxygen concentration (the regime of the undoped AF insulating state), we observe a nearly symmetrical transconductance curve of I_D versus V_G. The results shown in Fig. 1 are typical of a fully reduced YBCO channel. With increasing oxidation in the cuprate channel, we observe a monotonically increasing field-induced *p*-type and decreasing *n*-type mobility for a given magnitude of V_G.

Figure 2(a) shows similar dual-type transconductance of a second device. The on/off ratio, indicating the ratio of the drain current I_D with and without applied gate field, amounts to more than 10^4 for the *n*-type transconductance. The I_D vs V_D curves measured for different V_G show regular field-effect characteristics[6,12] for $V_G<0$ and $V_D<0$ [see Figs. 2(b) and 3]: a linear region with $I_D \propto V_D$ for $|V_D| \ll |V_G|$ and a saturation region $I_D(V_D) \approx$ const for $|V_D| \gg |V_G|$. This is also observed in other materials like monocrystalline, amorphous (*a*-Si), or polycrystalline Si (poly-Si), or in organic semiconductors. With $V_G>0$ and $V_D<0$ [see Fig. 2(c)], I_D increases monotonically with increasing V_D because there is no pinch-off effect[6,12] resulting from the fact that source and drain voltages have opposite polarities.

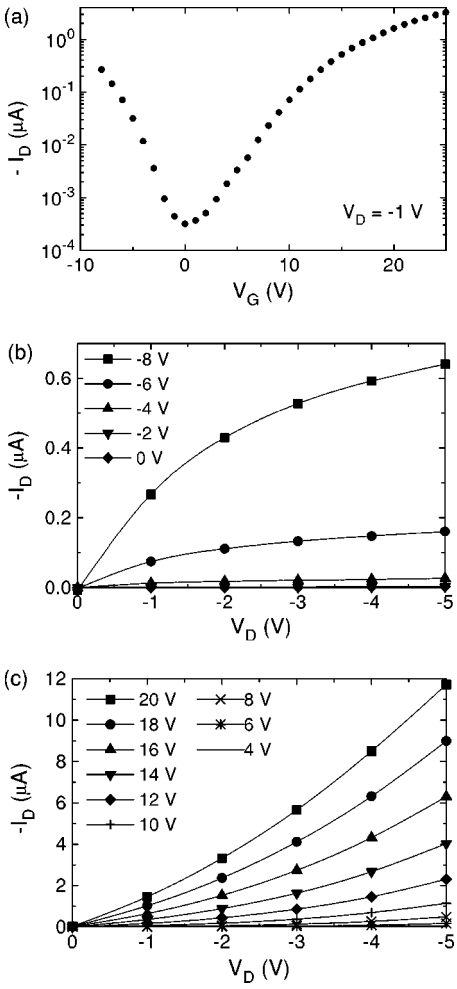

FIG. 2. (a) Semilogarithmic plot of the transconductance curve showing an on/off ratio of more than 10^4 in the *n* channel. The drain voltage V_D was set to -1 V. FET behavior for (b) different negative (0–−8 V) and (c) positive gate voltages (4–20 V) for the same device as in (a). The solid lines are a guide to the eye.

The overall field-effect behavior of our YBCO TFT samples can be fully explained using the orthodox model for FET's.[6,12] The field-effect mobility μ^{FE} of the carriers can be calculated in the linear region

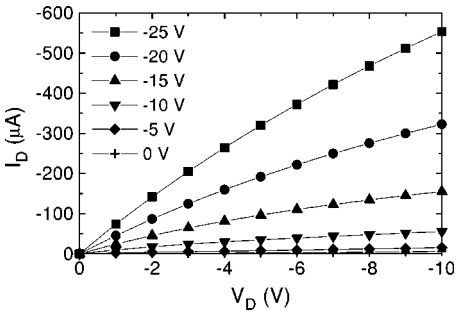

FIG. 3. FET characteristics of a device with higher oxygen content than that of the previous examples. The curves are for different V_G. The solid lines are a guide to the eye.

$$\mu^{\mathrm{FE}} = g \frac{l}{wC_s V_D}. \quad (2)$$

It is interesting to compare the field-effect mobility with the carrier mobility μ in optimally doped YBCO. We expect that $\mu^{\mathrm{FE}} < \mu$ for all gate voltages. Starting with a nearly undoped YBCO (see Fig. 1) we obtain a *p*-type field-effect mobility $\mu_p^{\mathrm{FE}}(V_G = -20\,\mathrm{V}) \approx 0.03\,\mathrm{cm}^2/\mathrm{V\,s}$, and an *n*-type mobility $\mu_n^{\mathrm{FE}}(V_G = 20\,\mathrm{V}) \approx 0.02\,\mathrm{cm}^2/\mathrm{V\,s}$ [Fig. 1(b)]. We always observe $\mu_p^{\mathrm{FE}} > \mu_n^{\mathrm{FE}}$ for the same magnitude of the gate field. With increasing oxygen content in the YBCO channel (and hence intrinsic hole concentration) μ_p^{FE} increases, whereas μ_n^{FE} decreases to 0. Figure 3 shows an example of a high *p*-type mobility $\mu_p^{\mathrm{FE}}(V_G = -25\,\mathrm{V}) = 0.88\,\mathrm{cm}^2/\mathrm{V\,s}$, which is comparable to values observed in *a*-Si or poly-Si. For optimally doped YBCO, the Hall mobility in the *a*-*b* plane μ_H has been estimated at room temperature to be about 4 $\mathrm{cm}^2/\mathrm{V\,s}$,[13] which is comparable to our rough estimate $\mu = (ne\rho)^{-1} \approx 7\,\mathrm{cm}^2/\mathrm{V\,s}$, where $n \approx 3 \times 10^{21}\,\mathrm{cm}^{-3}$, e is the elementary charge, and $\rho \approx 300\,\mu\Omega\,\mathrm{cm}$ in the *a*-*b* plane at room temperature. Our results in terms of mobility and field-induced carrier concentration show that the extended states with metallic conduction have not been reached yet.

Previous studies using YPBCO have shown comparable *p*-type but no *n*-type transconductance,[9–11] indicating that there is no significant *n*-type mobility in this compound. In order to study this issue in more detail, we have fabricated two FET's, one with a YPBCO channel ($y = 0.5$) and the other with a YBCO channel. After thin-film deposition, both samples have been annealed in the same way. Only the YBCO sample has shown finite *n*-type mobility. We note that another experiment,[14] using a YBCO channel, has indeed shown finite transconductance for both gate-field polarities at room temperature which has been ascribed to gate leakage. We have measured the gate leakage currents in our devices simultaneously with I_D, and for the data shown here, they have been at least one order of magnitude smaller than the drain currents for $V_G > 0$, thus excluding gate leakage as an artifact. Charge transport in several FET devices with underdoped YBCO channels has been studied between room temperature and 4.2 K by Milliken *et al.*[15] It is found that the temperature dependence of the channel conductance can be understood in terms of two-dimensional variable range hopping (VRH) for the case of zero applied V_G. The effect of enhancing the carrier concentration by applying gate voltage does not change the essential nature of the observed VRH conductance other than that the magnitude of the conductance increases and its temperature dependence decreases. All the results suggest charge transport in localized states.

IV. DISCUSSION

All our observations can be understood with a model based on electric-field-induced energy band bending of the channel material and a finite density of states within the band gap (see Fig. 4). This model was successfully employed in conjunction with amorphous[16] and organic[17] semiconductors. The intrinsic (chemical) doping concentration of the cuprate channel determines the level E_μ of chemical potential in the band structure.[1,2] To simplify the following discussion, we assume a two band model with a band gap of 1–2 eV. E_μ is at midgap in the undoped situation (Mott insulator). An increasing oxygen content will shift E_μ towards the lower band, thus increasing the density of carriers in the lower band (hole doping). It is important to recognize that there is a finite density of states $N(E)$ in the doped cuprates occupying the band gap as deduced from photoemission spectroscopy or optical conductivity experiments,[1,2] or the temperature dependence of our FET samples.[15] These states can be identified with, for example, localized states in self-organized nanograins in these doped antiferromagnetic insulators.[18,19] Recent experimental studies of the phonon linewidths in underdoped $YBa_2Cu_3O_{7-x}$ have confirmed the existence of dynamic charge segregation.[20]

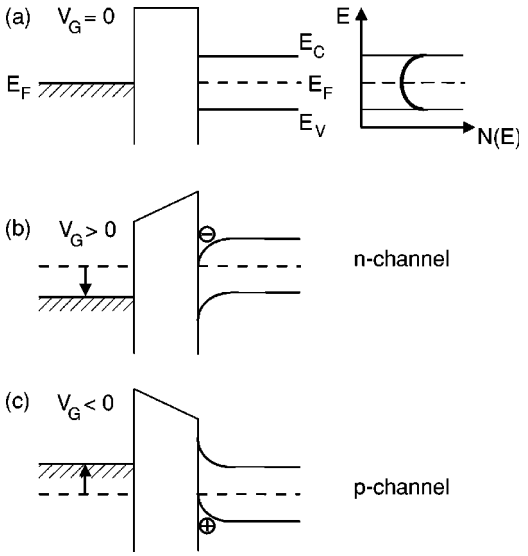

FIG. 4. Schematics of the cuprate FET band structure for (a) no, (b) positive, and (c) negative applied gate voltage. For each panel, there is shown from left to right: the metallic gate (with Fermi energy E_F), the dielectric gate insulator, and the cuprate active channel (with conductance-band edge E_C, Fermi energy E_F, and valence-band edge E_V). The density of states $N(E)$ within the band gap is schematically shown in the top right corner.

One might guess that crystal granularity or a rough STO/YBCO interface is responsible for the localized states. However, our samples consist of epitaxially grown films and, more importantly, the observed transconductance behavior is tuneable with chemical oxygen doping. This suggests an intrinsic mechanism such as charge granularity in the form of self-organized charge rich and charge poor domains, without dominating crystal granularity. Similar dual-type transconductance can be expected in nickelates and manganates, where the doped charges also reside in self-organized charge rich domains due to antiferromagnetic correlations of the undoped material. Indeed, such behavior apparently has been observed in $Nd_{0.7}Sr_{0.3}MnO_3$.[21]

The application of an electric field results in the bending of the bands; the direction of bending is determined by the polarity of the field. The bending occurs only at the surface of the cuprate, within the Thomas-Fermi screening length ($\approx$1 nm) of the electric field. Dual-type transconductance can occur for E_μ being at midgap, such that the applied electric field produces an accumulation of charge carriers irrespective of the field polarity. We expect that the details of

the dual-type transconductance depend on the energetic distribution of the localized states, which can vary slightly from sample to sample. We want to point out that complete symmetry can be observed only if the cuprate shows the following properties: E_μ is at midgap, the density of states within the band gap is symmetrical with respect to midgap, and electrons and holes possess the same effective mass and relaxation time. Any deviation from these criteria will result in asymmetrical transconductance characteristics.

In contrast, when the chemical potential is closer to the valence-band edge (*p*-doped sample), asymmetric characteristics and an approach to the relatively high mobility expected for the Mott insulator–metal transition are observed. In this chemical doping regime, $V_G<0$ further increases the concentration of mobile holes in the layer opposite the gate electrode, and hence increases the channel conductance. On the other hand, for $V_G>0$, depletion of carriers is expected for moderate fields, as is observed in our measurements. The maximum on/off ratio occurs for E_μ at midgap, where the channel resistivity is a maximum for $V_G=0$. A higher mobility but smaller on/off ratio occurs for finite chemical doping. Similar behavior has been observed in disordered organic semiconductors and was explained by variable-range hopping conduction between localized states.[22]

The observed gate-field dependence of the mobility is quite similar to that seen in organic FET's.[17] The current understanding of this behavior relies on the progressive filling of localized states with increasing $|V_G|$, resulting in simultaneously increasing μ^{FE}. Eventually, when all localized states are occupied by the induced carriers, additional charge goes into more extended states and therefore attains a high saturating mobility.[23] For the calculation of μ^{FE} (2) we assume C_s to be independent of V_G. Careful measurements of C_s indicate a slight relative variation of less than 30%, whereas μ^{FE} changes by more than an order of magnitude for the same swing of V_G. Therefore $C_s(V_G)=\mathrm{const}$ is a fair approximation, and the strong transconductance variation with V_G clearly reflects the change in μ^{FE} with the localized states with lowest μ^{FE} being at midgap.

Mobilities in organics in the range 0.05–0.1 $\mathrm{cm}^2/\mathrm{V\,s}$ have been attributed to the formation of extended current transporting states as a result of local self-organization, in contrast to the variable-range hopping of self-localized polarons found in more disordered polymers.[24] In the case of cuprates, in the extreme underdoped regime, the low mobility is related to variable-range hopping conduction, whereas higher doping concentration results in a larger mobility, which eventually leads to metallic conductivity (Mott transition) (see Refs. 2, 18, and 19 and references therein). It is important to recognize that in the case of organic semiconductors, E_μ is not at midgap due to finite (mostly *p*-type) doping, and that is why there is no observation of dual-type transconductance with organic FET's.

V. CONCLUSIONS

There are important implications of our observations for understanding the normal-state properties of the high-T_c superconductors. Applying an electric field opens up the possibility of investigating *n*-type doping in addition to *p*-type doping, thus allowing one to also explore the electron-doped side of the phase diagram. It is important, however, to recognize the subtle differences of the action of an electric field (electronic doping) and chemical doping. One obvious difference is the length scale of charge neutrality. In the case of chemical doping this length is of the order of the lattice unit, whereas for electronic doping the length is given by the thickness of the dielectric layer separating the cuprate from the gate electrode. In addition, the strong electric field, which is needed to significantly change the carrier concentration, can alter the detailed balance between the antiferromagnetic correlation energy, the Coulomb energy, and the kinetic energy, which control the spatial charge distribution.[25] Clearly, the electronic doping influences only a very thin layer of the cuprate channel due to the small Thomas-Fermi screening length. Therefore all results obtained with FET-type experiments can only yield information about various properties in this thin-film limit. This consideration is relevant regarding superconducting or other phenomena related to the phase diagram. Further studies are needed to clarify the details of the action of an electric field on stationary and dynamic charge behavior in the cuprates.

The dual-type transconductance offers new possibilities for applications of thin-film cuprate FET's, such as, for example: single device full-wave rectifiers, multilevel storage memory, complementary integrated circuits, complementary metal-oxide semiconductor-type logic gates, or interface amplifiers between high-T_c and room-temperature electronics employing the same cuprate material but with different doping level. Here, the cuprate offers several advantages compared to *a*-Si for instance, such as the compatibility to gate insulators with a high dielectric constant, a high uniformity of doping concentration on small length scales, or the integrability in three dimensions.[10] The performance can be further improved by decreasing the thickness of the gate dielectric or using a material with an even higher dielectric constant, thus enabling a smaller V_G to produce a similar transconductance.

ACKNOWLEDGMENTS

We thank C. D. Dimitrakopoulos, A. Gupta, R. H. Koch, F. P. Milliken, J. A. Misewich, and A. Schrott for stimulating discussions and G. Trafas for valuable technical assistance.

*Present address: Infineon Technologies AG, P.O. Box 800949, D-81609 Munich, Germany.

[1] E. Dagotto, Rev. Mod. Phys. **66**, 763 (1994).
[2] M. Imada, A. Fujimori, and Y. Tokura, Rev. Mod. Phys. **70**, 1039 (1998).
[3] C. C. Almasan and M. B. Maple, in *Chemistry of High Temperature Superconductors*, edited by C. N. R. Rao (World Scientific, Singapore, 1992), p. 205.
[4] J. E. Hirsch, Phys. Rev. B **50**, 3165 (1994).
[5] R. J. Gooding, K. J. E. Vos, and P. W. Leung, Phys. Rev. B **50**, 12 866 (1994).
[6] Y. Taur and T. H. Ning, *Fundamentals of Modern VLSI Devices* (Cambridge University Press, Cambridge, 1998).
[7] J. Mannhart, Supercond. Sci. Technol. **9**, 49 (1996).
[8] C. H. Ahn, S. Gariglio, P. Paruch, T. Tybell, L. Antognazza, and J.-M. Triscone, Science **284**, 1152 (1999).

[9] S. Hontsu, J. Ishii, M. Nakamori, H. Tabata, T. Kawai, and A. Fujimaki, IEEE Trans. Appl. Supercond. **7**, 3536 (1997).
[10] D. M. Newns, J. A. Misewich, C. C. Tsuei, A. Gupta, B. A. Scott, and A. Schrott, Appl. Phys. Lett. **73**, 780 (1998).
[11] D. M. Newns, T. Doderer, C. C. Tsuei, W. M. Donath, J. A. Misewich, A. Gupta, B. M. Grossman, A. Schrott, B. A. Scott, P. C. Pattnaik, R. J. Von Gutfeld, and J. Z. Sun, J. Electroceram. (to be published).
[12] S. M. Sze, *Physics of Semiconductor Devices* (Wiley, New York, 1981), Chap. 8.2.2.
[13] H. L. Stormer, A. F. J. Levi, K. W. Baldwin, M. Anzlowar, and G. S. Boebinger, Phys. Rev. B **38**, 2472 (1988).
[14] A. Levy, J. P. Falck, M. A. Kastner, W. J. Gallagher, A. Gupta, and A. W. Kleinsasser, J. Appl. Phys. **69**, 4439 (1991).
[15] F. P. Milliken, T. Doderer, R. H. Koch, and C. C. Tsuei (unpublished).
[16] G. W. Neudeck and A. K. Malhotra, J. Appl. Phys. **46**, 2662 (1975).
[17] G. Horowitz, Adv. Mater. **10**, 365 (1998).
[18] C. C. Tsuei and T. Doderer, Eur. Phys. J. B **10**, 257 (1999).
[19] T. Doderer and C. C. Tsuei, in *Advances in Solid State Physics*, edited by B. Kramer (Vieweg, Braunschweig, 1999), Vol. 39, p. 361.
[20] H. A. Mook and F. Doğan, Nature (London) **401**, 145 (1999).
[21] S. B. Ogale, V. Talyansky, C. H. Chen, R. Ramesh, R. L. Greene, and T. Venkatesan, Phys. Rev. Lett. **77**, 1159 (1996).
[22] A. R. Brown, C. P. Jarrett, D. M. de Leeuw, and M. Matters, Synth. Met. **88**, 37 (1997).
[23] C. D. Dimitrakopoulos, S. Purushothaman, J. Kymissis, A. Callegari, and J. M. Shaw, Science **283**, 822 (1999).
[24] H. Sirringhaus, N. Tessler, and R. H. Friend, Science **280**, 1741 (1998).
[25] V. J. Emery, S. A. Kivelson, and O. Zachar, Phys. Rev. B **56**, 6120 (1997), and references therein.